Measurement 129 (2018) 245–255

Contents lists available at ScienceDirect

Measurement

journal homepage: www.elsevier.com/locate/measurement

Speed control for K-mirror of 2-m telescope using improved active disturbance rejection controller

Yongting Deng[a], Peipei Xia[a,b,*], Hongwen Li[a], Xianjun Wang[a]

[a] Changchun Institute of Optics, Fine Mechanics and Physics, Chinese Academy of Sciences, Changchun 130033, China
[b] University of Chinese Academy of Sciences, Beijing 100049, China

ARTICLE INFO

Keywords:
Turntable of K-mirror
Speed control
Active disturbance rejection controller
Adaptive control law

ABSTRACT

To meet the high-precision requirements of the speed control system of the K-mirror of a 2-m telescope in terms of fast response, small overshoot, and strong anti-disturbance ability, a new active disturbance rejection controller (ADRC) based on the adaptive control law parameter is proposed. On the basis of the field rotation angle of the altitude-azimuth (alt-az) telescope and speed control performance requirements of the K-mirror turntable, an extended state observer is employed to estimate disturbances accurately from the input and output information of the system response. Then, the estimated values are used by the output side of the speed controller as a feed-forward compensation to eliminate the effects of the disturbances. However, the response of the turntable is slow when the speed is sufficiently low and its overshoot is large when the speed is sufficiently high. Thus, the performance of the K-mirror servo system is degraded and the high-precision requirements are not satisfied. Therefore, this paper proposes an adaptive scheme developed by designing the P-type gain of the feedback control law into a function, which can be automatically adjusted with a change in the system input speed. When the turntable of the K-mirror runs at a low speed, the proposed method produces a large P-type gain to accelerate the system's speed response. When the turntable runs at a high speed, the method suppresses the P-type gain and guarantees that the system has no overshoot. Experiments are conducted using a digital signal processor and a field-programmable gate array (FPGA)-based platform. The results show that the adaptive scheme fulfills the system requirements with the fastest speed response, minimizes the overshoot, and exhibits satisfactory anti-disturbance performance compared to the proportional-integral (PI) controller and ADRC.

1. Introduction

A large-aperture altitude-azimuth (alt-az) telescope finds applications in various fields, such as astronomical observation and monitoring, orbit determination, and image recognition [1]. The K-mirror, as a subsystem of the telescope system, is used to compensate for the field rotation (i.e., image rotation) caused by the frame structure of the alt-az telescope and the composite movement of the position and direction axes [2], in order to achieve real-time target recognition and image processing. To realize real-time target recognition and ensure good image quality after cancellation of image rotation, the speed control system of the K-mirror should exhibit fast speed response, small overshoot, strong anti-disturbance ability, and smooth running [3,4]. However, it is difficult to satisfy the high-precision requirements because the speed control system is inevitably affected by friction, cogging torque ripple, and parameter uncertainty during its operation [5]. Therefore, it is of practical significance to study control algorithms for improving the speed performance of the K-mirror servo control system.

Many such control algorithms have already been studied in detail [6–13]. In general, these algorithms can be categorized into two types: typical control and modern control. A proportional-integral (PI) controller and its derivatives are suitable candidates for many applications because of their theoretical simplicity and convenient debugging. Li [14] employed a PI controller by integrating an internal model into a speed loop, where the proportion and integral time constant were designed on the basis of the filter parameter λ, thereby realizing non-overshoot at high speed and stable operation even at a lowest speed of 15″/s. However, the internal model control design depends on precise forward and inverse models of the plant, which are impossible to acquire for most practical plants. Zhang [15] proposed a variable-structure PID controller, whose parameters can be modified according to the instantaneous error, allowing the telescope to reach the desired speed

* Corresponding author at: Changchun Institute of Optics, Fine Mechanics and Physics, Chinese Academy of Sciences, No. 3888 Dong Nanhu Road, Changchun, Jilin 130033, China.
E-mail address: peiwaer07@163.com (P. Xia).

https://doi.org/10.1016/j.measurement.2018.07.023
Received 26 September 2017; Received in revised form 3 July 2018; Accepted 10 July 2018
Available online 12 July 2018
0263-2241/

with maximum acceleration and without overshoot. However, the number of debugging parameters in this controller is seven, which makes the controller extremely complex and difficult to realize in practice. The modern control technology can improve the speed performance effectively. Song [16] designed an observer in the frequency domain for high-precision speed measurement with the smallest phase lag compared with some other estimators. However, this observer requires a precise mathematical model of the plant, which is difficult to obtain in practice.

By contrast, the active disturbance rejection controller (ADRC), developed by Prof. Jingqing Han [17], does not require a precise mathematical model; it can estimate the lumped disturbances accurately from the input and output information of the system response. The estimated values are used by the output side of the speed controller as a feed-forward compensation to eliminate the effects of the disturbances. This method can actively reject disturbances in its structure, providing a new way to improve the speed performance of the servo control system, and it has been widely used in many applications [18–23]. Thus, ADRC is simple, its parameters are highly adaptable, and the system can maintain its performance even in the presence of uncertainties, disturbances, or variations in the plant parameters. Conventionally, in two-order ADRC, the P-type gain is a constant [24]. However, for the K-mirror turntable of a 2-m telescope, which exhibits nonlinear characteristics and is affected by varying disturbances under different operating points, the ADRC method cannot always guarantee good performance. This paper presents and validates an adaptive scheme that synthesizes the adaptive control law and ADRC technique, and is implemented in the speed loop. The adaptive control law is introduced to increase the P-type gain with a decrease in speed, such that to accelerate the system's response ability; and vice versa, decrease the P-type gain with an increase in speed, such that to minimize the system's overshoot.

The remainder of this paper is organized as follows. Section 2 derives the patterns of rotation and the target of the K-mirror. Section 3 briefly explains the improved ADRC scheme. Section 4 describes experiments conducted to demonstrate the effectiveness of the proposed control scheme; the experimental results are presented and analyzed. Finally, Section 5 concludes the paper.

2. Field rotation angle of the alt-az telescope and target of the K-mirror turntable

2.1. Field rotation angle of the alt-az telescope

2.1.1. Object field rotation angle

When the alt-az telescope tracks objects, the orientation of the azimuth axis Z in the receiving end field of the telescope system remains unchanged, i.e., it does not change with the rotation of the altitude and azimuth axes of the telescope. However, owing to the earth's rotation, the telescope's azimuth axis is not coincident with the earth's polar axis. Thus, the dot (such as $\boldsymbol{\sigma_m}$: off-axis) image in the field rotates along with the telescope's azimuth axis, except for the dot (such as $\boldsymbol{\sigma}$: on-axis),which is located on the telescope's azimuth axis, causing rotation of the telescope's object field. As shown in Fig. 1, from time $\boldsymbol{t_1}$ to time $\boldsymbol{t_2}$, the orientation of the azimuth axis Z remains unchanged ($\boldsymbol{\sigma Z}$ and $\boldsymbol{\sigma Z'}$ and remain in the same direction) when the dot image $\boldsymbol{\sigma'_m}$ rotates through an angle $\boldsymbol{\theta_1}$ about the field center of $\boldsymbol{\sigma}$. To obtain the object field rotation angle in plane rectangular coordinates, $\boldsymbol{\theta_1}$ in spherical coordinates is transformed into $\boldsymbol{\theta'_1}$. For further details, readers may refer to Ref. [25].

2.1.2. View field rotation angle

The folding plane mirror in the telescope's coudé light path rotates relatively with the rotation of the altitude and azimuth axes of the telescope. Compared with the input vector of the telescope, the output vector rotates through a certain angle about the axis of the telescope, generating the telescope's view field rotation. As shown in Fig. 2(a), the K-mirror system is located behind the M6 mirror in the optical system of the 2-m main alt-az telescope, which passes through the reflectors M1, M2, and M3. M1 and M3 are oval mirrors with dimensions of 320 mm × 220 mm, and the angle between the normal directions of M1 and M3 and the K-mirror rotor is 60°. M2 is a round mirror with a diameter of 190 mm, and the angle between its normal direction and the K-mirror rotor is 90°.

The mirrors M4, M5, and M6 are reflex reflectors. The detailed main light path of the K-mirror component is shown in Fig. 2(b). The rotation of the image space field has the following characteristics:

1. The plane mirror M3 is fixed in the tube, and the cross section rotates along with the movement of the horizontal and vertical axes synchronously.
2. The installation locations of the plane mirrors M4, M5, and M6 are fixed relatively; they do not move along the horizontal axis but rotate around the vertical axis.

The alt-az coordinates (A, Z) are employed in this 2-m telescope, where A is the azimuth, measured from due north to due east and ranging from 0° to 360°, and it corresponds to rotation around the position axis. Z is the zenith distance, measured from the zenith to forward beneath and ranging from 0° to 90°; it corresponds to rotation around the direction axis. The field rotation caused by the composite movement of the position and direction axes is discussed below (assuming that the anticlockwise direction is positive when observed against the direction of light):

1. When the azimuth axis rotates, the azimuth angle A will change to ΔA during time Δt. Furthermore, the optical systems placed before the K-mirror will rotate around the azimuth axis. ΔA is positive when A increases; the azimuth axis rotates from due north to due east, and the outward light of M6 rotates anticlockwise. By contrast, ΔA is negative when A decreases and the outward light of M6 rotates clockwise. Thus, the relationship between the rotation angle θ_1 of M6's outward light and ΔA is

$$\theta_2 = +\Delta A \tag{1}$$

2. When the pitch axis rotates, the pitch angle of Z will change to ΔZ during time Δt. Furthermore, the optical systems placed before M3 will rotate around the pitch axis; therefore, there exists relative motion between the cross section of the optical component before and after M3, and light will rotate on reflectors M4, M5, and M6. ΔZ is positive if Z increases; the pitch axis rotates from the zenith to forward beneath. The inward light of M4 rotates clockwise, and the outward light of the mirror placed after M6 rotates anticlockwise. By contrast, ΔZ is negative when Z decreases; the inward light of M4 rotates anticlockwise, and the outward light of the mirror placed after M6 rotates clockwise. Thus, the relationship between θ_2 and ΔZ is

$$\theta_2 = -\Delta Z \tag{2}$$

Finally, we can obtain the relationship between θ_2 and ΔA and ΔZ as follows

$$\theta_2 = \Delta A - \Delta Z \tag{3}$$

2.1.3. Field rotation angle

In conclusion, the field rotation angle, including the object field rotation angle (caused by the frame structure of the alt-az telescope) and the view field rotation angle (caused by the composite movement of the position and direction axes) in the exit pupil of the telescope is

$$\theta^* = \theta_1' + \theta_2 = \theta_1' + \Delta A - \Delta Z \tag{4}$$

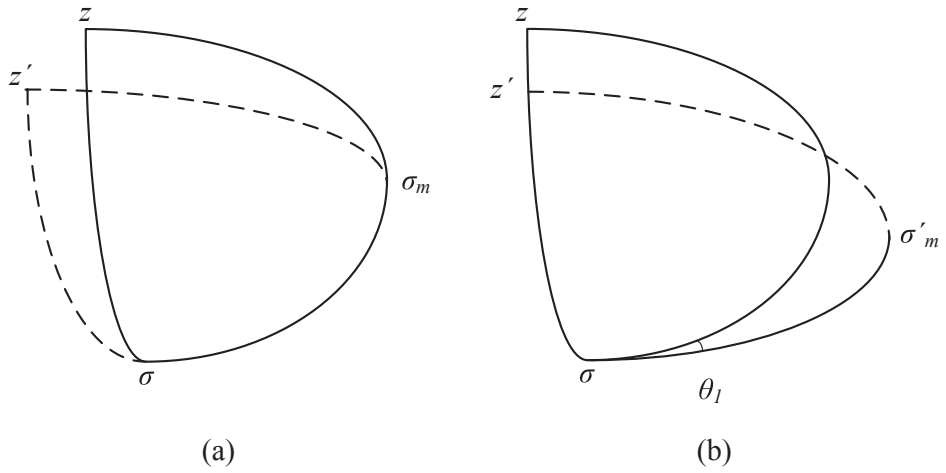

Fig. 1. Location of objects: (a) location in spherical coordinates; (b) location in the receiving end field.

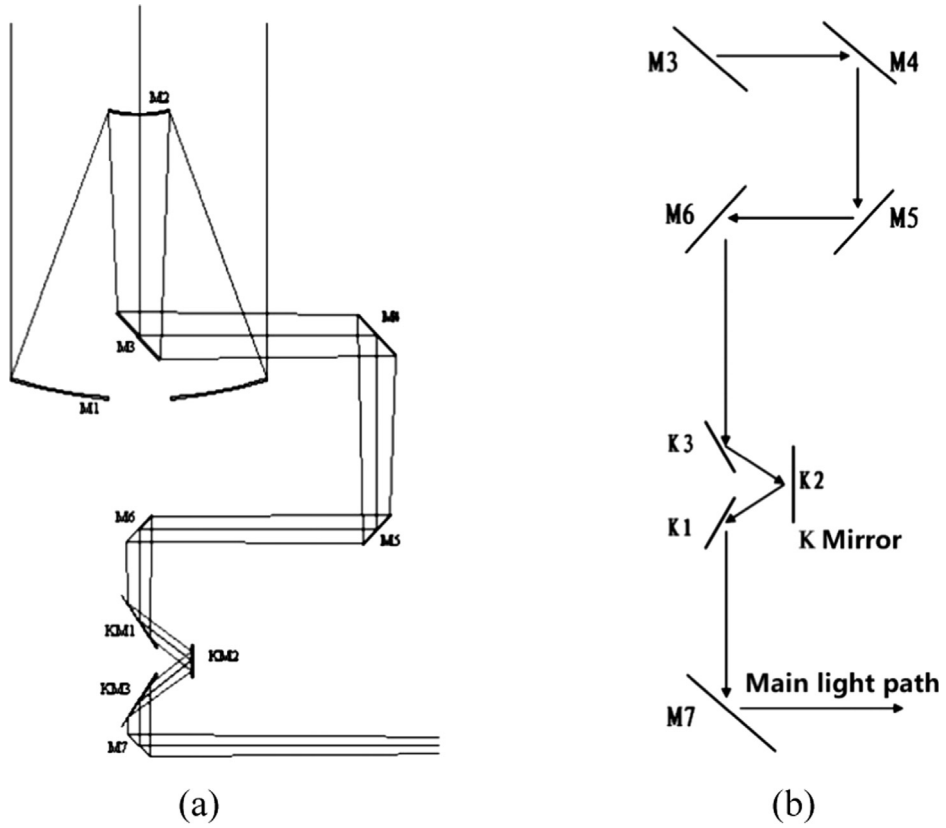

Fig. 2. Coudé light path: (a) optical system of the main alt-az telescope; (b) main light path of the K-mirror component of the 2-m alt-az telescope.

2.2. Requirements of speed control performance for the K-mirror turntable

It is known that when the rotational speed of the K-mirror is half of that of the inward light [2], the outward light imaging will have no rotation. Thus, to eliminate the field rotation of the telescope, the rotational speed of the K-mirror turntable should be set as (the calculation formula of the speed control performance)

$$\omega^* = \frac{1}{2}\frac{d\theta}{dt} = \frac{1}{2}\left(\frac{d\theta_1^{'}}{dt} + \frac{dA}{dt} - \frac{dZ}{dt}\right) \tag{5}$$

To eliminate the image rotation, the rotational speed ω^* is passed on as an instruction to the driving motor in order to drive the components of the K-mirror turntable.

With regard to the CCD camera having a resolution ratio of 1024×1024, the angle between two adjacent pixels, with respect to the center of imaging, *o*, as the origin and the farthest edge points, is $\sqrt{2}/1024 = 0.08^{\circ}$, i.e., the angular resolution ratio of the camera is 0.08°.

To ensure good image quality after de-rotation, the edge points of the image should be generated without overlap during single integration of the camera, the drive precision of the K-mirror axis should be much smaller than the angle between the two adjacent pixels on the edge of the image surface, and the accuracy of the position of the K-mirror axis should be at least

$$\theta^{'} = \sqrt{2}/1024 * 1/158 * 180/\pi * 3600 = 1.8'' \tag{6}$$

Calculating the speed in accordance with the long exposure ($t = 500$ ms), we can obtain the accuracy of the speed of the K-mirror

axis as follows (the specific target of the speed control performance)

$$\omega^{'} = d\theta^{'}/dt = 3.6^{''}/\mathrm{s} \tag{7}$$

Moreover, the maximum overshoot of the speed should not exceed 1% during the work scope of 0°/s to 10°/s, and the transit time of steady tracking should not exceed 2 s.

3. Design of adaptive ADRC

The ADRC method is an "active" control technology that views exogenous and endogenous disturbances as "lumped disturbances" and extends the total disturbance as a new state; the disturbance is estimated using the extended state observer (ESO) in real time and the estimated value is fed forward to the controller output to actively compensate for the disturbances. Because of this advantage (active rejection of disturbances), the ADRC algorithm is applied to the servo control system of the K-mirror turntable. Furthermore, considering the large variation in the disturbance characteristics during different motion states, the P-type controller parameter of the feedback control law is designed into a function, which is automatically adjusted with a change in the system's input speed. When the K-mirror turntable runs at a low speed, the parameter of the P-type control law is appropriately magnified to improve the compensation capabilities of the system in order to accelerate the system's speed response. By contrast, when the K-mirror turntable runs at a high speed, the parameter of the P-type control law is suitably decreased to avoid the large overshoot caused by the saturation controller in order to further improve the system's dynamic performance. The schematic of adaptive ADRC is shown in Fig. 3.

In practice, the servo system of the K-mirror turntable uses the DC torque motor to be driven directly. By ignoring the mechanical resonances and small time constant inertia units at high frequency, we can simplify the mathematical model of the DC torque motor as

$$G_p(s) = \frac{k}{(T_m s + 1)(T_e s + 1)} \tag{8}$$

where k is the open-loop gain of the system, T_m is the mechanical time constant and T_e is the electric time constant. The servo system of the K-mirror turntable is a large rotational inertia system, where T_m is much larger than T_e; therefore, we can ignore the influence of T_e, and thus, Eq. (8) can be further simplified as

$$G_p(s) = \frac{k}{(T_m s + 1)} \tag{9}$$

3.1. Design of ADRC

The simplified mathematical model in Eq. (9) can be described as the equation of state as follows:

$$\begin{cases} \dot{x}_1 = bu + f(t, y(t), d(t)) \\ y = x_1 \end{cases} \tag{10}$$

where $d(t)$ is the exogenous disturbance, $f(t, y(t), d(t)) = d(t) - \frac{1}{T_m} y(t)$ is the total disturbance including internal and external disturbances, and $b = \frac{k}{T_m}$ is the coefficient from the control input u to acceleration $\dot{y}$.

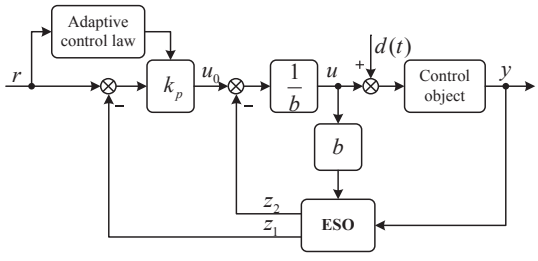

Fig. 3. Topology of ADRC based on adaptive control law parameter.

Treating $f(t, y(t), d(t))$ as an additional state variable $x_2 = f$, we can extend the origin plant in Eq. (10) as

$$\begin{cases} \dot{x}_1 = bu + f(t, y(t), d(t)) \\ \dot{x}_2 = \dot{f} \\ y = x_1 \end{cases} \tag{11}$$

Now, we construct a two-order state observer, denoted as the ESO, in the form of

$$\begin{cases} e = z_1 - y \\ \dot{z}_1 = z_2 - \beta_1 e + bu \\ \dot{z}_2 = -\beta_2 e \end{cases} \tag{12}$$

where z_1 is the estimated value of the output speed y of the system, z_2 is the estimated value of the total disturbance f of the system, and β_1 and β_2 are the gains of the ESO.

There are many ways to choose the observer gains of β_1 and β_2 [26]. To simplify the implementation, the observer gains can be made linear. For example, the observer gains in Eq. (12) can be selected as [27]

$$\begin{cases} \beta_1 = 2\omega_0 \\ \beta_2 = \omega_0^2 \end{cases} \tag{13}$$

where ω_0 is the bandwidth of the ESO.

The control law of u with disturbance compensation is given as

$$u = \frac{u_0 - z_2}{b} \tag{14}$$

From Eq. (14), it can be found that the ADRC control method contains a linear disturbance feed-forward compensation item $-b^{-1}z_2$, which is estimated by the linear ESO. The ESO is designed to estimate the disturbance online and add a corresponding feedback compensation item to the control input, thus the ADRC control method can get a strong anti-disturbance capability.

Besides, it is observed from Eq. (12) that the inputs to the ESO are the system output $y$and control signal u, and the output of the ESO gives important information of f. This allows the control law $(u_0 - z_2)/b$ to convert the plant in Eq. (10) into the following cascade integral form

$$\begin{cases} \dot{x}_1 = u_0 - z_2 + f \approx u_0 \\ y = x_1 \end{cases} \tag{15}$$

which is considerably simplified and can easily be controlled.

The integral control method is applied to a traditional PI controller in order to eliminate the steady-state error caused by the step input and constant disturbance. However, Eq. (15) shows that the plant is reduced to a structure with "pure integration"; therefore, integral control is not necessary in the controller of u_0 to avoid the problem of slow response and phase lag caused by the integrator [28]. Then, the P-type controller is adopted as follows [24,29]

$$u_0 = k_p(r - z_1) \tag{16}$$

where k_p is the gain of the control law and r is the reference speed.

By substituting Eq. (15) into Eq. (16), we can describe the plant as the following transfer function

$$G_{close} = \frac{y(s)}{r(s)} = \frac{k_p}{s + k_p} \tag{17}$$

3.2. Design of adaptive control law

Within a certain speed range, keeping the parameter k_p in Eq. (16) constant, the servo system of the K-mirror turntable can acquire a good control effect through the traditional ADRC method. However, because of the existence of dead zones when the K-mirror turntable runs at an extremely low speed (such as 0.001°/s), although the ESO can estimate the value of f, the turntable cannot respond in a timely manner because the output code values of the P-type controller are less than the

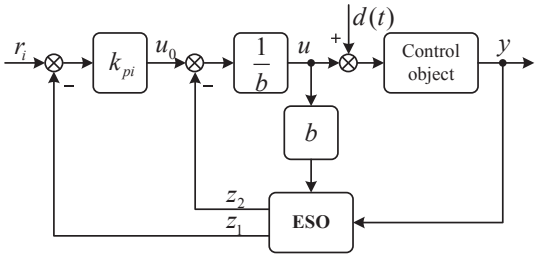

Fig. 4. Block diagram of ADRC scheme.

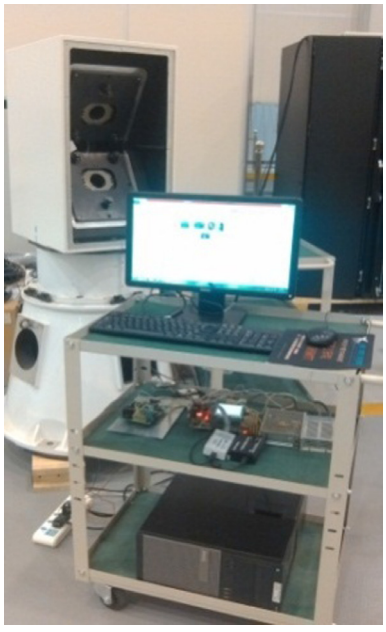

Fig. 5. Physical map of the experimental platform.

Table 1
DC torque motor parameters.

Description	Value
Rotary inertia J	9.7×10^{-2} kg·m^2
Torque constant K_t	7.33 N·m/A
Armature inductance L	0.021 H
Armature resistance R	8.5 Ω

threshold of the dead zones. Hence, the system cannot compensate for the friction torque in real time, leading to a slow speed response. By contrast, when the K-mirror turntable runs at a high speed (such as 10°/s), the output code value of the P-type controller with a fixed parameter is saturated, leading to a large overshoot value (62%), and hence, a longer time to enter the stable state. Therefore, the requirements of the speed control system of the K-mirror can only be met by solving the problems of "controlling small dead zones" and "controlling large overshoot".

Given these problems, in this study, we designed the gain of the P-type controller into a function, where the reference speed is viewed as an independent variable and the gain is adjusted automatically with a change in input speed. The gain k_p of the P-type controller, is increased suitably with automatic reduction of the input speed signal in order to strengthen the compensation ability. Otherwise, k_p is decreased suitably with an automatic increase in the input speed signal to avoid the generation of oscillation and controller saturation and to minimize the overshoot and shorten the adjustment time. The process is carried out in the following steps:

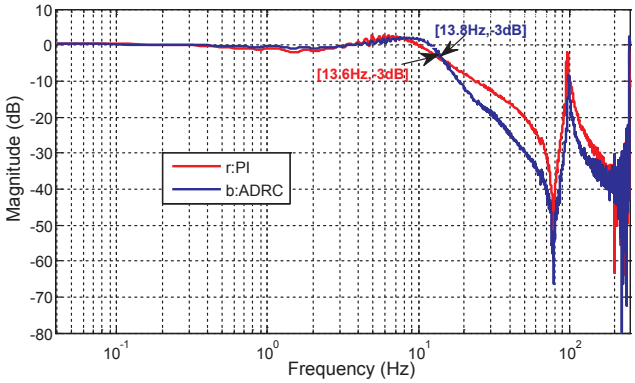

Fig. 6. Comparison results of the closed-loop Bode diagrams under the PI and ADRC methods.

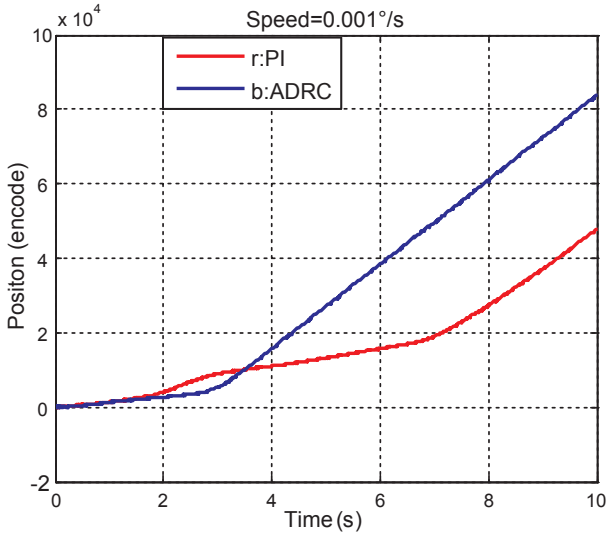

Fig. 7. Comparison results of position curves at a speed of 0.001°/s under the PI and ADRC methods.

1. The control scheme is shown in Fig. 4, given that the speed testing points of r_1, r_2, …, r_n, respectively, obtain the control law parameters k_{p1}, k_{p2}, …, k_{pn} at the moment when the control characteristics reach their optimal state.
2. Based on the optimal control law parameters, the regression analysis method is adopted [30], and based on the least sum of squares of deviations principle, the adaptive law between the P-type controller gain k_p and the reference speed r is established, i.e., $k_p = f(r)$, which ensures that the system rejects the disturbance furthest and the dynamic performance of the system is improved. The discrete data of k_{pi} correspond to r_i, the fitting function is $f(r_i)$, and the accuracy of the fitting can be expressed as

$$d(r_i) = |k_{pi} - f(r_i)| \tag{18}$$

The fitting function is regarded as the model of control law parameters when the value of Eq. (19) is the smallest.

$$E = \sum_{i=1}^{n} d^2(r_i) \tag{19}$$

4. Experimental results and analysis

The effectiveness of the proposed adaptive ADRC scheme is verified experimentally. A photograph of the experimental platform is shown in Fig. 5.

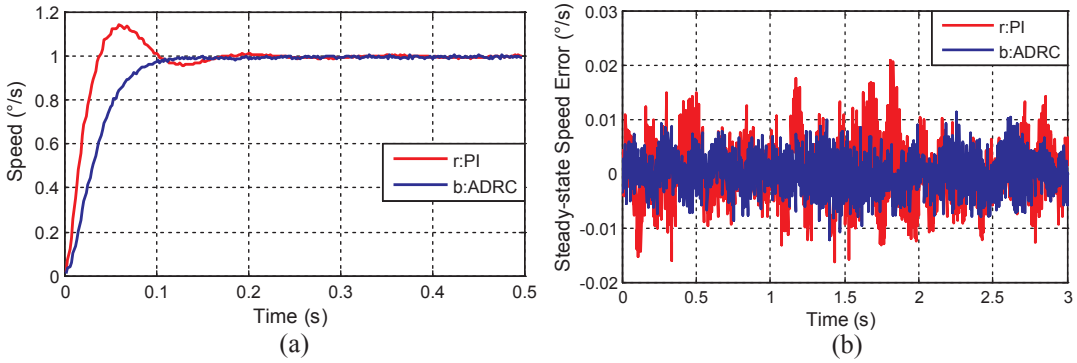

Fig. 8. Comparison results of the speed control performance at a speed of 1°/s under the PI and ADRC methods: (a) comparison results of the step response; (b) comparison results of the steady-state speed error.

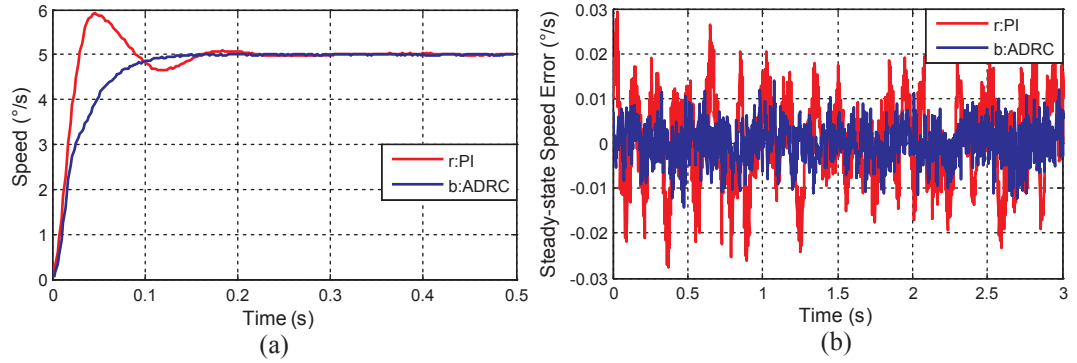

Fig. 9. Comparison results of the speed control performance at a speed of 5°/s under the PI and ADRC methods: (a) comparison results of the step response; (b) comparison results of the steady-state speed error.

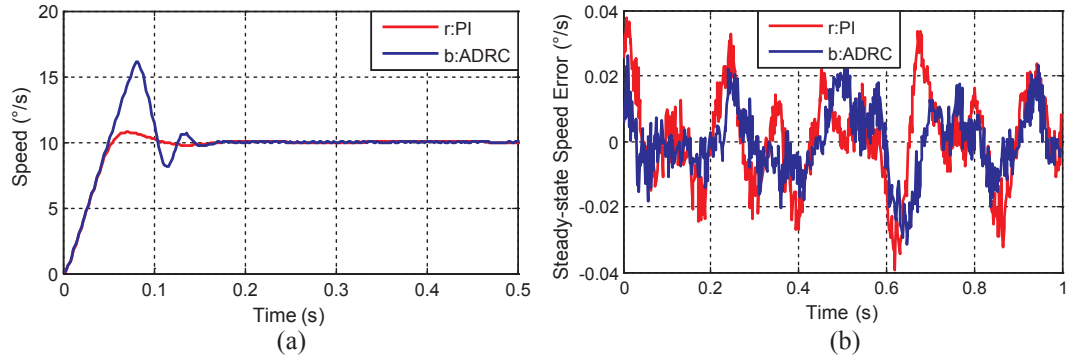

Fig. 10. Comparison results of the speed control performance at a speed of 10°/s under the PI and ADRC methods: (a) comparison results of the step response; (b) comparison results of the steady-state speed error.

According to the system requirements of the 2-m alt-az telescope, the maximum acceleration of the telescope azimuth axis is $\alpha_1 = 5°/s^2$ and that of the zenith axis is $\alpha_2 = 3°/s^2$; thus, the maximum acceleration of the rotation axis of the K-mirror turntable is $\alpha_{max} = \alpha_1 + \alpha_2 = 8°/s^2$. On the basis of the mechanical design of the K-mirror turntable, the weight of the K-mirror turntable is less than 150 kg and the rotating radius is less than 300 mm. In consideration of the resistance torque N_f generated by the bearing and electric cable, we can estimate the rotary inertia J of the K-mirror turntable and the maximum torsional torque N_{max} required for its rotation as follows: $N_{max} = J\alpha_{max} + N_f$ [31]. According to the value of the maximum torsional torque N_{max}, a permanent-magnet DC torque motor (model J300LYX02A) having a radius of 200 nm is employed. In addition, a Renishaw absolute encoder having an external diameter of 255 mm is employed. The detailed parameters of the permanent-magnet DC torque motor are listed in Table 1.

The proposed overall control scheme is realized on the hardware platforms of DSP-TMS320F28335 (a 150-MHz processor) and FPGA-EP3C40F324 [32] (a 100-MHz processor with 39,600 logic elements). The proposed algorithm is implemented in a primary controller, i.e., a digital signal processor (DSP), using a C program, and it provides speed loop control instructions. A field-programmable gate array (FPGA) is used as the secondary controller to realize the functions of pulse-width modulation and generation, communication, and speed acquisition. The PWM digital control signal is magnified by an intelligent power module (IPM) IPM-PS21A79 [33] (its specified nominal voltage and current are 600 V and 50A, respectively; the maximum PWM input frequency is 20 kHz) into an energetic signal in order to drive the turntable rotation according to the instructions. A 32-bit absolute encoder is employed to evaluate the digital position. The correcting frequency of the speed loop is 500 Hz. The carrier frequency of the PWM is 10 kHz.

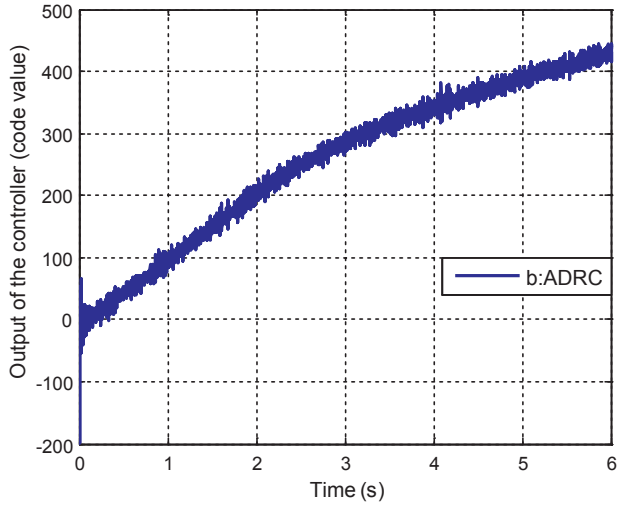

Fig.11. Output code value of controller at a speed of 0.001°/sunder the ADRC method.

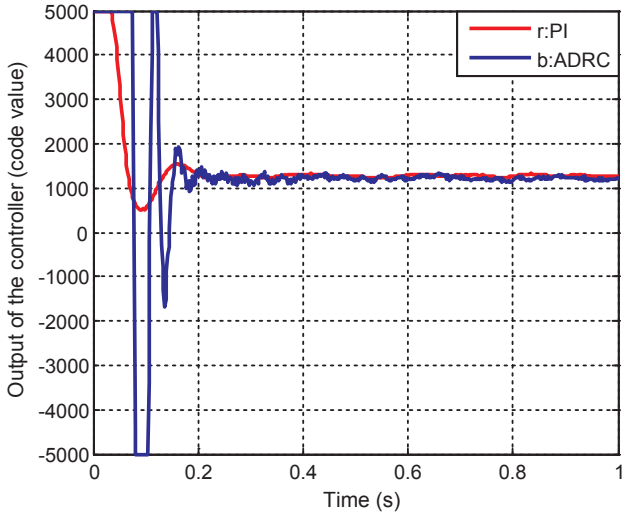

Fig.12. Output code value of controller at a speed of 10°/sunder the PI and ADRC methods.

Table 2
Experimental results of the optimal control law parameters at the speed testing point.

Reference speed (°/s)	0.005	0.01	0.05	0.1	0.5	1	2	5	8	10
Optimal value of k_p	249	170	134	110	114	95	90	61	48	36

4.1. Problems of "controlling small dead zones" and "controlling large overshoot"

According to the analysis described above, we know that the parameter $b = k/T_m$ is the parameter that we should determine from the control model first. Because the load and DC torque motor are coupled, we cannot obtain the plant's transfer function through the motor parameters theoretically. In this study, we determine k and T_m by using the data of the open-loop response, where T_m is the time when the system's output value reaches 0.632 of the steady-state value of the objects and k is the ratio of the output steady value and input steady value [34,35]. Considering that the "dead zone" phenomenon exists in the system because of friction and rotary inertia, we need to perform open-loop experiments repeatedly. The various control values of u, such as $[u_1 \quad u_2 \cdots u_n]$, are input into the system, and the respective responses

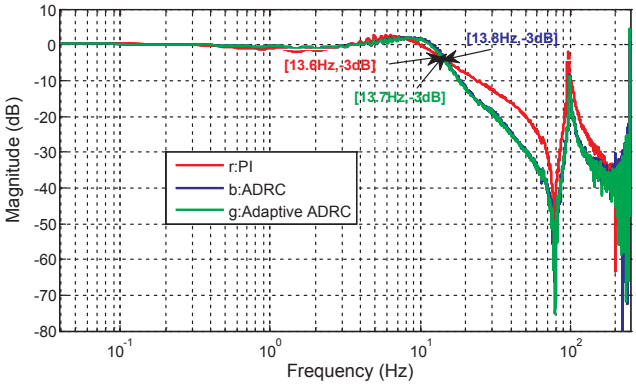

Fig.13. Comparison results of the closed-loop Bode diagrams under the PI, ADRC, and adaptive ADRC methods.

of the steady-state value $[\omega_1 \quad \omega_2 \cdots \omega_n]$ are recorded. We assume that

$$\omega = k(u - D) \tag{20}$$

where D is the threshold of the dead zone. The turntable will respond only if the control value of u is greater than the threshold of dead zone$D$.

The transfer function between the input control value u and the output angular speed$\omega$is roughly obtained as

$$G_p(s) = \frac{0.0307}{0.55s + 1} \tag{21}$$

Further, the threshold of dead zone D is

$$D = 312 \tag{22}$$

To investigate the effectiveness of ADRC in terms of the dynamic performance under different operating speed conditions, experiments are carried out at 0.001°/s (extremely low speed), 1°/s and 5°/s (middle speed), and 10°/s (high speed), using the PI and ADRC methods.

To ensure fair comparison, the parameters of the PI and ADRC methods are selected under the same speed closed-loop bandwidth conditions. The closed-loop Bode diagrams under the PI and ADRC methods are shown in Fig. 6. It is observed from the experimental results that the closed-loop system exhibits similar -3 dB bandwidths compared to the PI and ADRC methods, which are 13.6 and 13.8 Hz, respectively.

The parameters of the PI and ADRC speed controllers are $k_p = 0.05$, $k_i = 0.005$; and $\omega_0 = 60$, $k_p = 96$, respectively.

At an extremely low speed of 0.001°/s, the signal was flooded with noise; thus, we give the curve of the position at a speed of 0.001°/s in this paper. The experimental results of the position curves at a speed of 0.001°/s under the PI and ADRC methods are shown in Fig. 7. It is observed from the experimental results that, in the PI method, at an extremely low speed, the settling time is 7.3 s, whereas in the ADRC method, the settling time is 3.2 s. Thus, the dynamic response ability is better under the ADRC method compared to the PI method. However, neither control method can meet the system requirement in terms of the settling time (the settling time should not exceed 2 s).

The experimental results of the speed control performance at speeds of 1°/s and 5°/s under the PI and ADRC methods are shown in Figs. 8 and 9, respectively. From the experimental results shown in Fig. 8, it is observed that at a speed of 1°/s, in the PI method, the overshoot is 14.5% and the settling time is 0.25 s, whereas in the ADRC method, there is no overshoot and the settling time is 0.13 s. Further, from the experimental results presented in Fig. 9, it is observed that at a speed of 5°/s, in the PI method, the overshoot is 18.8% and the settling time is 0.22 s, whereas in the ADRC method, there is no overshoot and the settling time is 0.12 s. Moreover, it is observed that, at speeds of both 1°/s and 5°/s, the steady-state speed error shows a smaller amplitude under the ADRC method compared to the PI method. Thus, the

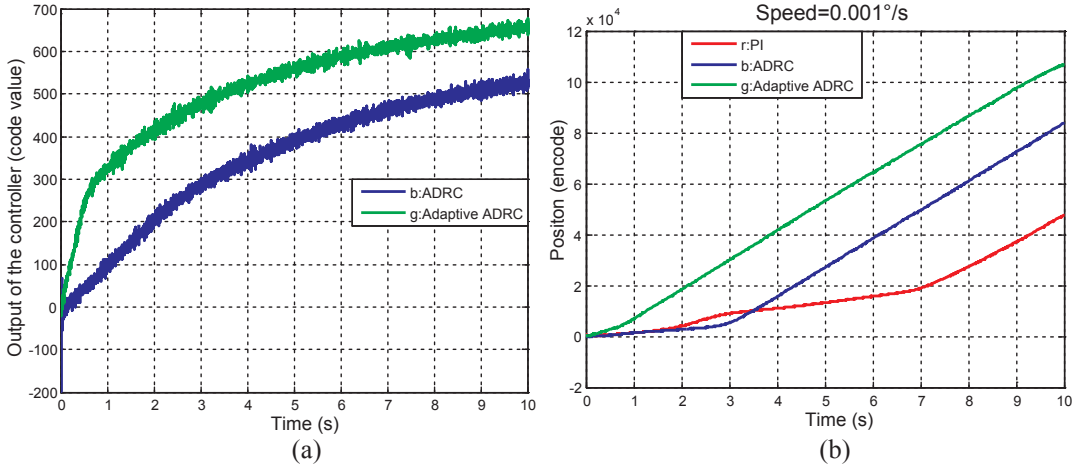

Fig. 14. Comparison results of the output at a speed of 0.001°/s under the PI, ADRC, and adaptive ADRC methods: (a) comparison results of the controller output code value; (b) comparison results of the position curves.

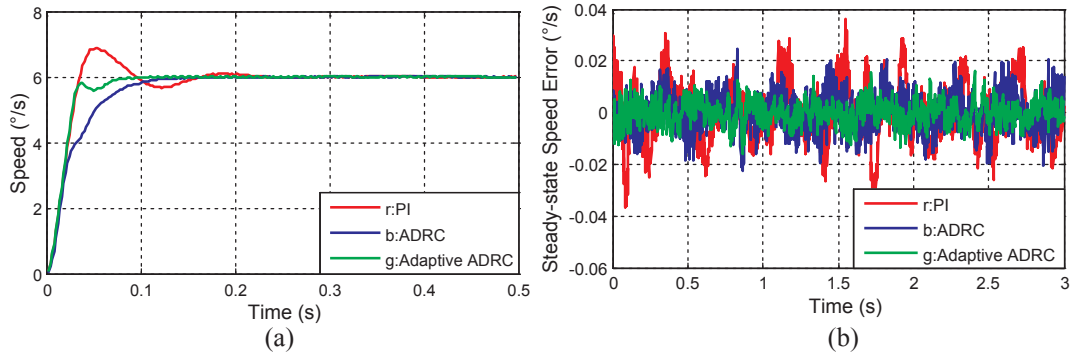

Fig. 15. Comparison results of speed control performance at a speed of 6°/s under the PI, ADRC, and adaptive ADRC methods: (a) comparison results of the step response; (b) comparison results of the steady-state speed error.

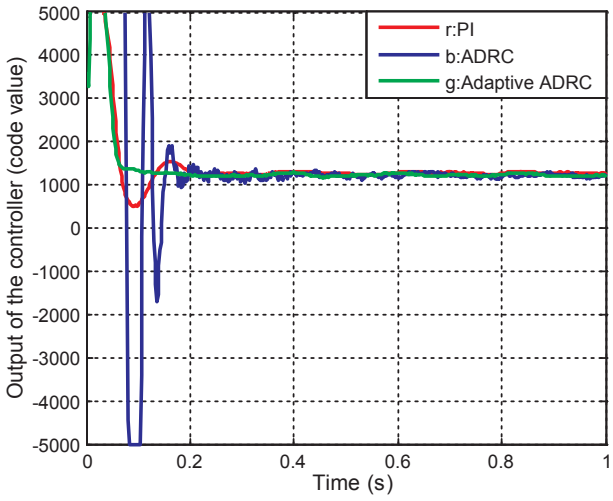

Fig. 16. Output code value of controller at a speed of 10°/s under the PI, ADRC, and adaptive ADRC methods.

effectiveness of the ADRC in terms of the dynamic and steady-state performance is verified at speeds of 1°/s and 5°/s.

The experimental results of speed control performance at a speed of 10°/s under the PI and ADRC methods are shown in Fig. 10. Fig. 10(a) shows the results of the speed step response and Fig. 10(b) shows the results of the steady-state speed error. From the experimental results presented in Fig. 10(a), it is observed that at a speed of 10°/s, in the PI method, the overshoot is 8% and the settling time is 0.25 s, whereas in the ADRC method, the overshoot is 62% and the settling time is 0.22 s. Further, from the experimental results presented in the Fig. 10(b), it is observed that the steady-state speed error shows a smaller amplitude under the ADRC method compared to the PI method.

According to the experimental results presented above, we can conclude that, at some speed, the speed control performance under the ADRC method is better than that under the PI method. However, problems occur at extremely low speeds (0.001°/s) and high speeds (10°/s). To meet the system's requirements, we should improve the system control performance further. First, we must determine some of the aspects that might contribute to the poor performance; thus, we study the output code values of the controller.

The controller output code values at a speed of 0.001°/s under the ADRC method are shown in Fig. 11. It is observed from the experimental results that, at an extremely low speed, the output code value of the ADRC method is less than the threshold of dead zone D in the initial 3.2 s; hence, the power amplifier devices can neither overcome the dead zone nor further drive the turntable to respond. Therefore, the disturbance cannot be compensated in real time.

The controller output code values at a speed of 10°/s under the PI and ADRC methods are shown in Fig. 12. It is observed from the experimental results that the output code values of the PI and ADRC methods generate the phenomenon of saturation, which can degrade the system's dynamic performance.

According to the experimental results of the controller output code values, it is observed that the system's control performance can be improved if we can solve the problems of "controlling small dead zones" and "controlling large overshoot". Thus, the adaptive ADRC

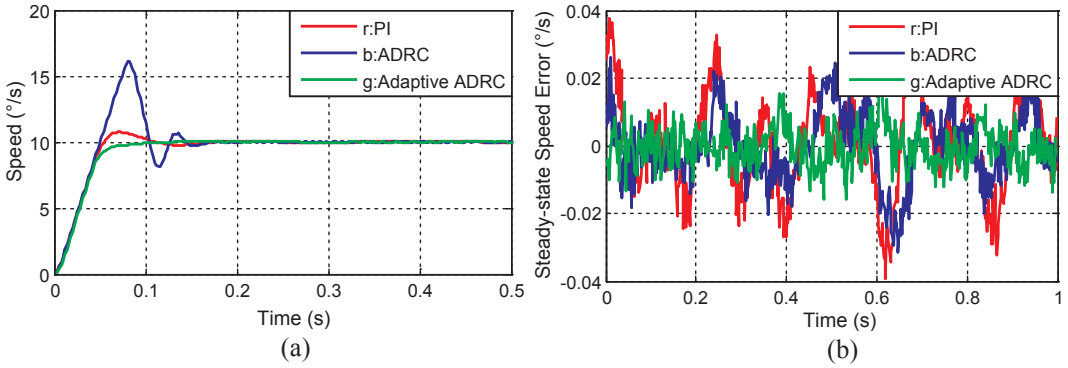

Fig. 17. Comparison results of speed control performance at a speed of 10°/s under the PI, ADRC, and adaptive ADRC methods: (a) comparison results of the step response; (b) comparison results of the steady-state speed error.

Table 3
Experimental results of dynamic and steady-state performance.

Speed (°/s)	Control Method	Overshoot (%)	Settling time (s)	RMSvalue of steady-state speed error (°/s)
1	PI	14.5	0.25	0.0055
	ADRC	No	0.13	0.0048
	Adaptive ADRC	No	0.06	0.0038
5	PI	18.8	0.22	0.0092
	ADRC	No	0.12	0.0053
	Adaptive ADRC	No	0.07	0.0042
6	PI	16.7	0.22	0.0113
	ADRC	No	0.19	0.0070
	Adaptive ADRC	No	0.08	0.0042
10	PI	8	0.25	0.0123
	ADRC	62	0.22	0.0065
	Adaptive ADRC	No	0.1	0.0033

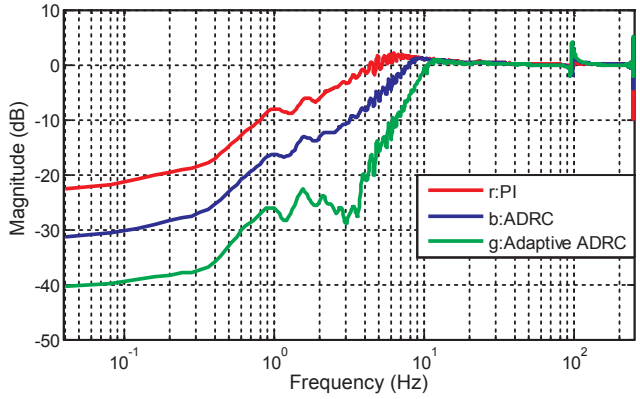

Fig.18. Comparison results of the Bode diagram of the disturbance's transfer function under the PI, ADRC, and adaptive ADRC methods.

method is proposed.

4.2. Experiments for adaptive control law

On the basis of the design method of the adaptive feedback control law proposed in Section 3.2, we carried out an experimental study to obtain the optimal feedback control law parameters under various operating speeds. The experimental results of the optimal control law parameters at the speed testing point are summarized in Table 2. According to the experimental results, it is observed that the system achieves optimal control performance under different values of k_p.

On the basis of the experimental results of the optimal control law parameters, the following functional relationship is established between k_p and r:

$$k_p = \begin{cases} 249 & |r| \leqslant 0.005 \\ \frac{629.2*abs(r)+2.473}{r^2+5.082*abs(r)-0.00647} & |r| > 0.005 \end{cases} \quad (23)$$

From Eq. (23), it can be observed that with the speed input r increased, the gain k_p in the adaptive ADRC method is less than that in the ADRC method, which indicates that with the system input increased, the less gain k_p is good for suppressing the "controlling large overshoot". On the other hand, with r decreased, the gain k_p in the adaptive ADRC method is more than that in the ADRC method, which indicates that with the system input decreases, the gain k_p gradually increases to overcome the "controlling small dead zone". Thus, the controller designed by the proposed adaptive law can dynamically adapt to the variation of the speed input r, and compensate the disturbance in real time. Based on the above analysis, the adaptive ADRC method can get a better dynamic response performance and a stronger anti-disturbance capability compared with the ADRC method.

4.3. Effectiveness of adaptive ADRC in terms of step response under different operating speed conditions

To investigate the effectiveness of adaptive ADRC in terms of the dynamic performance under different operating speed conditions, experiments are carried out at 0.001°/s, 6°/s, and 10°/s, using the PI, ADRC, and adaptive ADRC methods.

To ensure fair comparison, the parameters of the PI, ADRC, and adaptive ADRC methods are selected under the same speed closed-loop bandwidth conditions. The closed-loop Bode diagrams under the PI, ADRC, and adaptive ADRC methods are shown in Fig. 13. It is observed from the experimental results that the closed-loop system exhibits similar −3dB bandwidths compared with the PI, ADRC, and adaptive ADRC methods, which are 13.6, 13.8, and 13.7 Hz, respectively.

The parameters of the PI, ADRC, and adaptive ADRC speed controllers are $k_p = 0.05$, $k_i = 0.005$; $\omega_0 = 60$, $k_p = 96$; and $\omega_0 = 60$, $k_p = f(r)$, respectively.

The controller output code values at a speed of 0.001°/s under the ADRC and adaptive ADRC methods are shown in Fig. 14(a). It is observed from the experimental results that the adaptive ADRC method can suitably increase k_p on the basis of the input reference speed, making the controller's output code value greater than the threshold of dead zone D after 0.9 s; thus, the power amplifier devices can overcome the dead zone and drive the turntable to respond. Therefore, the disturbance can be compensated in a timely manner and the dynamic performance of the system can be further improved. The experimental results of the position curves at a speed of 0.001°/s under the PI, ADRC,

and adaptive ADRC methods are shown in Fig. 14(b). It is observed from the experimental results that, in adaptive ADRC method, the settling time is further reduced to 0.9 s. Thus, we can conclude that the adaptive ADRC method can solve the problem of "controlling small dead zones" and meet the system requirements in terms of the settling time.

The experimental results of the speed control performance at a speed of 6°/s under the PI, ADRC, and adaptive ADRC methods are shown in Fig. 15. Fig. 15(a) shows the results of the speed step response and Fig. 15(b) shows the results of the steady-state speed error. From the experimental results presented in Fig. 15(a), it is observed that at 6°/s, in the PI method, the overshoot is 16.7% and the settling time is 0.22 s; in the ADRC method, there is no overshoot and the settling time is 0.19 s; and in the adaptive ADRC method, there is no overshoot and the settling time is further reduced to 0.08 s. Moreover, from the experimental results presented in Fig. 15(b), it is observed that for the speed steady-state error, in the PI method, the amplitude is 0.0113, whereas in the ADRC and adaptive ADRC methods, the amplitudes are reduced to 0.007 and 0.0042, respectively.

Thus, we can conclude that the adaptive ADRC method can improve the dynamic performance and reduce the steady-state speed error of the system. In addition, the speed of 6°/s is not the speed of the speed testing point; k_p is obtained through the adaptive control law. From the experimental results presented in Fig. 15, it is observed that the proposed control law is correct and effective.

The controller output code values at a speed of 10°/s under the PI, ADRC, and adaptive ADRC methods are shown in Fig. 16. It is observed from the experimental results that the output code value of the adaptive ADRC method can suitably decrease k_p on the basis of the input reference speed, making the system enter the steady state without overshoot after 0.1 s.

The experimental results of the speed control performance at a speed of 10°/s under the PI, ADRC, and adaptive ADRC methods are shown in Fig. 17. Fig. 17(a) shows the results of the speed step response and Fig. 17(b) shows the results of the steady-state speed error (obtained after the settling time). From the experimental results presented in Fig. 17(a), it is observed that at a speed of 10°/s, in the PI method, the overshoot is 8%; in the ADRC method, the overshoot is 62%; and in the adaptive ADRC control, there is no overshoot. Furthermore, from the experimental results presented in Fig. 17(b), it is observed that the steady-state speed error shows the smallest amplitude under the adaptive ADRC method compared to the PI and ADRC methods. Thus, we can conclude that the adaptive ADRC method can solve the problem of "controlling large overshoot" and meet the system requirements in terms of small overshoot while improving the accuracy of the steady-state speed error of the system.

The experimental results of the settling time, overshoot, and steady-state speed error in the speed step response of the three methods are summarized in Table 3. It is observed that, compared to the ADRC method, in the adaptive ADRC method, at a speed of 1°/s, the settling time is shortened by 53.8% and the steady-state speed error RMS value is reduced by 20.8%. Further, at a speed of 5°/s, the settling time is shortened by 41.6% and the steady-state speed error RMS value is reduced by 20.7%. In addition, at a speed of 6°/s, the settling time is shortened by 57.8% and the steady-state speed error RMS value is reduced by 40%. Finally, at a speed of 10°/s, the settling time is shortened by 54.5% and the steady-state speed error RMS value is reduced by 49.2%.

The experimental results of the speed control performance presented above verify the effectiveness of the proposed adaptive ADRC scheme in improving the dynamic and steady-state performance under various speed conditions.

4.4. Verification of anti-disturbance ability of adaptive ADRC

To evaluate the anti-disturbance ability of the adaptive ADRC scheme, the closed-loop frequency characteristics of the disturbance's transfer function are tested. The Bode diagrams of the disturbance's transfer function under the PI, ADRC, and adaptive ADRC methods are shown in Fig. 18. It is observed from the experimental results that at high frequencies, the amplitude-frequency characteristics of the three methods are in good agreement. However, in the range of middle-low frequencies of 0.1–10 Hz, the anti-disturbance ability improves by 23 dB under the adaptive ADRC method compared to the PI method. Thus, we conclude that the anti-disturbance ability is improved significantly under the adaptive ADRC method compared to the PI and ADRC methods.

5. Conclusion

To improve the control precision of the K-mirror of a 2-m, a strategy was proposed by using the adaptive ADRC. The adaptive feedback control law based on the input in the adaptive ADRC, was designed to solve the problem of "controlling small dead zone" and "controlling large overshoot" in the ADRC method. In addition, the ESO was applied to estimate the uncertain system disturbances, and the estimated value was designed as a feedback item to compensate for the input of adaptive ADRC. This proposed adaptive ADRC method could achieve the desired control of the system with external disturbances. The effectiveness of the proposed method was verified by comparing the experimental results with those derived using the traditional method.

References

[1] J.X. Zhang, Overview of structure technologies of large aperture ground-based telescopes, Chin. Opt. 5 (4) (2012) 327–336 (in Chinese).
[2] Z.C. Wang, Y.Z. Zhao, C. Zhou, Design of K mirror for Alt-az telescope, Acta Photon. Sin. 41 (7) (2012) 762–765 (in Chinese).
[3] P. Guo, Study of telescope's derotation system (Ph.D. Dissertation), Changchun Institute of Optics, Fine Mechanics and Physics, Chinese Academy of Sciences, Changchun, 2013, pp. 12–58 (in Chinese).
[4] Y. Zhang, J.X. Zhang, B.G. Chen, et al., Design of support structure for K mirror, Laser Optoelectron. Prog. 52 (2015) 062203(1-6). (in Chinese).
[5] Y.T. Deng, H.W. Li, J.L. Wang, et al., Main axes AC servo control system for 2m telescope, Opt. Precis. Eng. 25 (1) (2017) 163–171 (in Chinese).
[6] P. Dasari, L. Alladia, A.S. Raoa, et al., Optimal H2-IMC based PID controller design for multivariable unstable process, IFAC-Pap Online 49 (1) (2016) 617–622.
[7] Y.J. Zhang, J. Zhang, L. Wang, et al., Composite disturbance rejection control based on generalized extended stateobserver, ISA Trans. 63 (7) (2016) 377–386.
[8] B. Tamhane, D. Singh, S. Kurode, et al., Observer based control of a missile seeker system using sliding modes: seeker system, Asian J. Control 18 (2) (2016) 784–787.
[9] Q. Wang, C. Lu, W. Pan, IMC PID controller tuning for stable and unstable process with time delay, Chem. Eng. Res. Des. 105 (2016) 120–129.
[10] G. Sun, X. Ren, D. Li, Neural active disturbance rejection control output control of multimotor servomechanism, IEEE Trans. Control Syst. Technol. 23 (2) (2015) 746–753.
[11] Y. Zou, X. Lei, A compound control method based on the adaptive neural network and sliding mode control for inertial stable platform, Neurocomputing 155 (2015) 286–294.
[12] W.K. Gawronski, C.S. Racho, J.A. Mellstrom, Application of the LQG and feed-forward controllers to the deep space network antennas, IEEE Trans. Control Syst. Technol. 3 (4) (1995) 417–421.
[13] W.T. Wang, J. Guo, Z.H. Jiang, et al., Application of linear active disturbance rejection control for photoelectric tracking system, High Tecnol. Lett. 23 (3) (2017) 315–321 (in Chinese).
[14] H.W. Li, Servo system of large telescope based on internal model PID control method, Opt. Precis. Eng. 17 (2) (2009) 327–332 (in Chinese).
[15] B. Zhang, H.W. Li, L.H. Guo, et al., Application of variable structure PID in velocity control for large telescope, Opt. Precis. Eng. 18 (7) (2010) 1613–1619 (in Chinese).
[16] Y. Song, H.B. Gao, S.M. Zhang, The analysis and design of low velocity estimation based on observer, Proceedings of the IEEE, International Conference on Automation and Logistics, Shenyang, China, (2009).
[17] J.Q. Han, From PID to active disturbance rejection control, IEEE Trans. Ind. Electron. 56 (3) (2009) 900–906 (in Chinese).
[18] Du. Bochao, Wu. Shaopeng, Shouliang Han, et al., Application of linear active disturbance rejection controller for sensorless control of internal permanent-magnet synchronous motor, IEEE Trans. Ind. Electron. 63 (5) (2016) 3019–3027.
[19] Nanfang Yang, Fei Gao, Damien Paire, et al., Distributed control of multi-time scale DC microgrid based on ADRC, IET Power Electron. 10 (3) (2017) 329–337.
[20] Dazi Li, Pan Ding, Zhiqiang Gao, Fractional active disturbance rejection control, ISA Trans. 62 (2016) 109–119.
[21] Nanfang Yang, Fei Gao, Damien, et al., Distribute control of multi-time scale DC microgrid based on ADRC, IET Power Electron. 10 (3) (2017) 329–337.

[22] Shweta Balajiwale, H. Arya, A. Joshi, Study of performance of ADRC for longitudinal control of MAV, IFAC-Papers online 49 (1) (2016) 585–590.
[23] P. Teppa Garran, G. Garcia, Design of an optimal PID controller for a coupled tanks system employing ADRC, IEEE Latin Am. Trans. 15 (2) (2017) 189–196.
[24] Jie Li, Yuanqing Xia, Xiaohui Qi, et al., On the necessity, scheme and basis of the linear-nonlinear switching in active disturbance rejection control, IEEE Trans. Ind. Electron. 64 (2) (2017) 1425–1435.
[25] Qinghua Ju, Study on Field Rotation of 1.2m Alt-Az Telescope and Elimination of Image-Rotation, University of Chinese Academy of Sciences, 2008 (in Chinese).
[26] J. Han, Active Disturbance Rejection Control Technique-the Technique Forestimating and Compensating the Uncertainties, Nat. Defense Ind. Press, Beijing, China, 2008.
[27] Zhiqiang Gao, Scaling and bandwidth-parameterization based controller tuning, Proceedings of the 2003, ACC, 2003, pp. 4989–4996.
[28] Zhiqiang Gao, On the foundation of active disturbance rejection control, Control Theory Appl. 30 (12) (2013) 1498–1510.
[29] Jie Li, Yuanhui Qi, Yuanqing Xia, et al., On linear/ nonlinear active disturbance rejection switching control, Acta Autom. Sini. 46 (2) (2016) 202–212.
[30] Lu Ning, The problem of successive functions to approach to the dispersed data, J. Northwestern Inst. Architect. Eng. 1 (1993) 41–46 (in Chinese).
[31] Peng Guo, Study of Telescope's Derotation System, Changchun Institute of Optics, Fine Mechanics and Physics, Chinese Academy of Sciences, 2013 (in Chinese).
[32] Yongting Deng, Hongwen Li, Jianli Wang, et al., Design of telescope servo system based on DSP and FPGA, Infrared Laser Eng. 43 (3) (2014) 908–914 (In Chinese).
[33] Hongwen Li, Jianli Wang, The current situation and development trend of theodolite servo power drives, Electron. Opt. Control 13 (2) (2006) 105–108 (in Chinese).
[34] J. Chen, Study on the low velocity properties and jitter compensation for the servo system (Ph.D. dissertation), Changchun Institute of Optics, Fine Mechanics and Physics, Chinese Academy of Sciences, 2001, pp. 66–68 (in Chinese).
[35] S.S. Hu, Automatic Control Principle, Science Press, 2012, pp. 73–75 (in Chinese).